IEEE Access
Multidisciplinary | Rapid Review | Open Access Journal

Received June 30, 2019, accepted July 24, 2019, date of publication July 29, 2019, date of current version September 11, 2019.

Digital Object Identifier 10.1109/ACCESS.2019.2931747

Improved Current Decoupling Method for Robustness Improvement of LCL-type STATCOM Based on Active Disturbance Rejection Control

MINGLEI WANG[1], XIANGYU WANG[2], JINXIN QIAO[1], AND LIGUO WANG[1]
[1]School of Electrical Engineering and Automation, Harbin Institute of Technology, Harbin 150001, China
[2]School of Electrical Engineering and Information, Northeast Petroleum University, Daqing 163318, China

Corresponding author: Liguo Wang (532882524@qq.com)

This work was supported in part by the Harbin Science and Technology Innovation Talent Research Special Fund under Grant RC2017LX007003.

ABSTRACT When theoretically studying the control method of LCL-type static synchronous compensator (STATCOM), we often ignore the influence of complex power grid on the stability and reactive compensation performance of STATCOM. Improving traditional current decoupling method with PI controller (PI decoupling) in synchronous (dq) reference frame, an original current decoupling method with active disturbance rejection controller (ADRC decoupling) is proposed in this paper. First, the influence of internal and external disturbances on STATCOM with PI decoupling method is analyzed. External disturbances include harmonic grid voltage and grid inductance variation. Internal disturbances come from coupled channels between d axis and q axis, and parameter perturbations of LCL filter. Second, the principle of ADRC decoupling method applied to LCL-type STATCOM is analyzed in detail. Taking advantage of ADRC's capability to estimate and compensate for the ''total disturbances'', robustness of STATCOM is improved. Comparing with PI decoupling method, ADRC decoupling method can improve the disturbances rejection performance and stability of LCL-type STATCOM. Finally, results from STATCOM simulation model show the effectiveness and superiority of this original method.

INDEX TERMS Active disturbance rejection controller (ADRC), current decoupling, external disturbances, internal disturbances, LCL-type STATCOM.

I. INTRODUCTION

STATCOM is utilized to compensate reactive power and stabilize the voltage at the point of common coupling (PCC) [1], [2]. With the development of renewable power generations, power grid disturbances such as voltage harmonics and grid inductance variation should not be ignored any more [3]–[7]. Compared with the L filter, the LCL filter has better performance to filter high order harmonic current, but its coupled channels between d axis and q axis are more complex in synchronous reference frame. Sometimes, traditional PI decoupling method for LCL-type STATCOM is unstable under the influence of power grid disturbances [3]. Disturbances from coupled channels between d axis and q axis would reduce the accuracy of reactive compensation current [8]. The above disturbances bring challenges to the traditional PI decoupling method for LCL-type STATCOM. The original decoupling method with stronger robustness is the focus of our study.

ADRC proposed by Han is an advanced and original control method [9]. ADRC can solve the contradiction between overshoot and dynamic response time, and it has better control performance at complex and changeable conditions. Furthermore, compared with PI controller, ADRC doesn't need accurate and detailed mathematical model of the controlled object, it has been applied to many industrial fields [10]–[14]. In [10], ADRC and iterative learning control are utilized to control robot finger's joins for assisting patients

The associate editor coordinating the review of this article and approving it for publication was Giambattista Gruosso.

to do rehabilitation training. In [11], the ADRC with self-adjusting parameters algorithm is proposed to suppress the disturbances and improve the tracking performance for continuous casting mold. In the field of electrical engineering, ADRC is studied and applied to maximize the wind power extraction in the wind farm consisted of direct-driven permanent magnet synchronous generator [12]. At the same time, ADRC can also be utilized to achieve multi-time scale control for DC microgrid [13], and applied to sensorless control of internal permanent-magnet synchronous motors [14]. On the other hand, some improved ADRC are proposed to obtain better control effect [15], [16].

Direct current control methods with PI controller are applied in LCL-type grid-connected inverter [17]–[19], but these control methods ignore the coupled channels between active current axis (d axis) and reactive current axis (q axis) in synchronous reference frame. In contrast, current decoupling control method has higher control accuracy, shorter dynamic response time and better disturbance rejection performance by removing the coupled channels [8], [5], [20]–[22]. In [21], PI decoupling method is applied for H-bridge cascaded STATCOM. But the achievement of decoupling relies on the accurate and detailed mathematical models of controlled object. When the value of grid inductance changes greatly, traditional PI decoupling method has unstable problems [5]. Current decoupling method without grid voltage feedforward control has poor disturbance rejection performance to suppress the influence of harmonic grid voltage [4]. In [22], ADRC combined with virtual synchronous generator control is proposed to achieve power fluctuations attenuation and system dynamic response improvement. In [23], ADRC is utilized to achieve active damping control and suppress the influence of harmonic grid voltage on output current for grid-connected inverter. In [24], ADRC is applied to obtain clustered balance for DC/DC converter. Decoupling method with ADRC can remove the coupled channels of controlled system with multiple inputs and multiple outputs, and it can improve the robustness for LCL-type STATCOM to reject internal and external disturbances. ADRC decoupling method is applied for LCL-type grid-connected inverter to achieve independent control of active current and reactive current. But the influence of complex power grid is ignored [25].

Based on the above analysis, in this paper, the influence of internal and external disturbances on traditional PI decoupling method is theoretically derived and analyzed in section II. The conclusion shows that PI decoupling method has poor performance under the influence of internal and external disturbances. In section III, The linear ADRC is utilized to replace the PI controller and achieve current decoupling control for STATCOM. The internal linear expansion state observer (LESO) is used to estimate accurately the system state variables and ''total disturbances'' in real time. The linear state error feedback controller (LSEF) is used to provide disturbances compensation and improve the dynamic response speed. The disturbance rejection performance is analyzed by comparing with traditional PI decoupling method. In section IV, based on MATLAB/Simulink simulation software, the LCL-type STATCOM simulation model is built to verify the effectiveness and superiority of the proposed ADRC decoupling method under different working conditions. The simulation results are consisted with the theoretical analyses.

II. PRINCIPLE ANALYSIS OF LCL-TYPE STATCOM

A. CONFIGURATION OF LCL-TYPE STATCOM

A LCL-type STATCOM connected to power grid is shown in Fig. 1. Where, U_{dc} is DC capacitor voltage; $u_{ia,b,c}$ are three-phase output voltage of inverter-side; $i_{1a,b,c}$ are three-phase output current of inverter-side; $i_{ca,b,c}$ are three-phase capacitor current; R_c is reactive damping resistor; $i_{2a,b,c}$ are three-phase enter-grid current; $u_{ca,b,c}$ are three-phase capacitor voltage; C_{dc} is DC capacitor; L_1, L_2, C are filter parameters; L_g is power grid inductance.

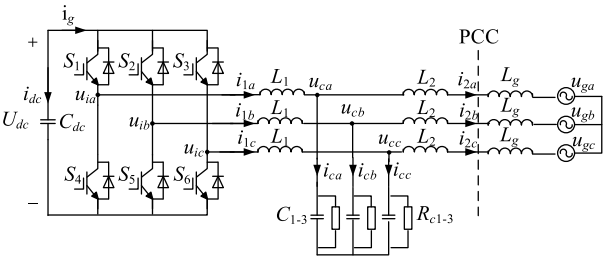

FIGURE 1. Configuration of LCL-type STATCOM connected to power grid.

B. MATHEMATICAL MODELS OF LCL-TYPE STATCOM

According to Fig. 1, the mathematical models of LCL-type STATCOM are derived in three-phase (abc) coordinate frame, they are shown in (1).

$$\begin{cases} L_1 \dfrac{di_{1k}}{dt} = u_{ik} - u_{ck} \\ (L_2 + L_g) \dfrac{di_{2k}}{dt} = u_{ck} - u_{gk} \qquad k = a, b, c \\ C \dfrac{du_{ck}}{dt} + \dfrac{u_{ck}}{R_c} = i_{1k} - i_{2k}, \end{cases} \tag{1}$$

S_k is a flag for indicating the switching state of IGBT on the inverter bridge. $S_k = 1$ when IGBT on the upper bridge arm is turned off and IGBT on the lower bridge arm is turned on; $S_k = 0$ when the situation is reversed. Mathematical models of LCL-type STATCOM in synchronous reference frame are shown in (2) by abc/dq transformation. By $Laplace$ transformation, equivalent block diagram of (2) is shown in Fig. 2. Where, ω_1 is fundamental angle frequency. The whole block diagram shows the characteristics of multiple variables and multiple coupled channels.

Figure. 2 has a symmetrical structure. Considering that the role of q axis is to control output reactive current, we choose q axis as the research object. The ''total disturbances'' include internal disturbances from $\omega_1 L_1 i_{1d}$, $\omega_1 C u_{cd}$ and $\omega_1 L_2 i_{2d}$; external disturbances from u_{gq} and L_g. Internal disturbances cause influence via coupled channels between d axis and

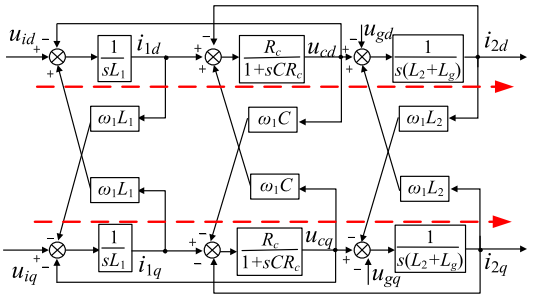

FIGURE 2. Block diagram of LCL-type STATCOM in *dq* reference frame.

q axis. In addition to considering the influence of i_{1d}, u_{cd} and i_{2d}, the parameter perturbations of the LCL filter caused by complex power grid conditions also need to be considered. On the other hand, external disturbances bring some problems such as instability and increased total harmonic distortion (THD) of reactive compensation current. Traditional PI decoupling method with large computation is difficult to obtain excellent control effect under the influence of the internal and external disturbances.

$$\begin{cases} \dfrac{di_{1d}}{dt} = \dfrac{u_{id} - u_{cd} + \omega_1 L_1 i_{1q}}{L_1} \\ \dfrac{di_{1q}}{dt} = \dfrac{u_{iq} - u_{cq} - \omega_1 L_1 i_{1d}}{L_1} \\ \dfrac{di_{2d}}{dt} = \dfrac{u_{cd} - u_{gd} + \omega_1 \left(L_2 + L_g\right) i_{2q}}{L_2 + L_g} \\ \dfrac{di_{2q}}{dt} = \dfrac{u_{cq} - u_{gq} - \omega_1 \left(L_2 + L_g\right) i_{2d}}{L_2 + L_g} \\ \dfrac{du_{cd}}{dt} = \dfrac{R_c i_{1d} - R_c i_{2d} + R_c \omega_1 C u_{cq} - u_{cd}}{CR_c} \\ \dfrac{du_{cq}}{dt} = \dfrac{R_c i_{1q} - R_c i_{2q} - R_c \omega_1 C u_{cd} - u_{cq}}{CR_c} \end{cases} \tag{2}$$

C. ANALYSIS OF INTERNAL AND EXTERNAL DISTURBANCES

The process of PI decoupling method is introduced in Fig. 21. In order to introduce the problems of PI decoupling method under the influence of internal and external disturbances, we take the q axis as the controlled object. PI controller is employed. The control block diagram is shown in Fig. 3. The total disturbances are marked in red.

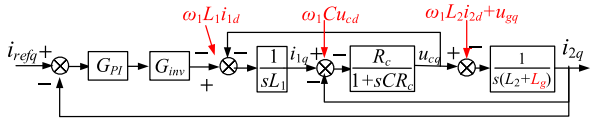

FIGURE 3. Control block diagram of *q* axis with PI controller for LCL-type STATCOM.

Where, i_{refq} is the reference current; PI controller is $G_{PI} = K_p + K_i/s$. Parameters are shown in Table 1. When the switching frequency is high enough, $G_{inv} = U_{dc}/U_{tri}$. Where, U_{tri} is the triangle carrier wave amplitude of the SPWM. Taking $G_{inv} = 330$ for theoretical analysis.

TABLE 1. Parameters for disturbance analysis.

Parameter/Unit	Value	Parameter/Unit	Value
Inverter-side inductor L_1/mH	5.5	Damping resistor R_c/Ω	3
Gird-side inductor L_2/mH	0.6	PI parameter K_p	0.45
Capacitor C/μF	6.6	PI parameter K_i	800

Single disturbance analysis method is used to analysis the influence of each disturbance.

1) INFLUENCE OF POWER GRID INDUCTANCE

According to Fig. 3, supposing that there is only disturbance L_g, closed-loop transfer function from i_{refq} to i_{2q} is derived:

$$D_{Lg}(s) = \frac{R_c K_p G_{inv} s + R_c K_i G_{inv}}{R_c C L_1 (L_2 + L_g) s^4 + L_1 (L_2 + L_g) s^3 + R_c (L_1 + L_2 + L_g) s^2 + R_c K_p G_{inv} s + R_c K_i G_{inv}} \tag{3}$$

Figure. 4 is the pole-zero map of (3). When L_g increases, the poles will enter the unstable region. So traditional PI decoupling method doesn't have enough robustness and stability when the power grid inductance changes.

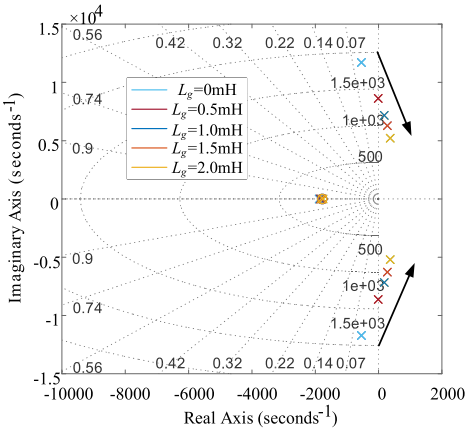

FIGURE 4. Pole-zero map of (3) when L_g changes.

2) INFLUENCE OF HARMONIC POWER GRID VOLTAGE

Supposing that there is only disturbance u_g similarly, closed-loop transfer function from u_{gq} to i_{2q} is derived too.

$$D_{ug}(s) = -\frac{R_c C L_1 s^3 + L_1 s^2 + R_c s}{R_c C L_1 L_2 s^4 + L_1 L_2 s^3 + R_c (L_1 + L_2) s^2 + G_{inv} R_c K_p s + G_{inv} R_c K_i} \tag{4}$$

According to Table 1, the magnitude of K_i is much larger than K_p. Ignoring items of small magnitude, (5) can be

derived by simplifying (4).

$$D_{ug\_simple}(s=j2\pi f_1) = -\frac{s}{G_{inv}K_i}|_{s=j2\pi f_1} = -\frac{j2\pi f_1}{G_{inv}K_i} \quad (5)$$

where, f_1 is the frequency of reactive compensation current, and $f_1 = 50$Hz. Vector diagram of error caused by u_g is shown in Fig. 5. Where, i_{refq} is reference component in i_{2q}; i_{ugq} is disturbance component in i_{2q}. $i_{ugq} = 0$ in the absence of grid voltage disturbances. The disturbances of the grid voltage cause the influence of output reactive compensation current on phase and amplitude, it can increase the THD of i_{2q}.

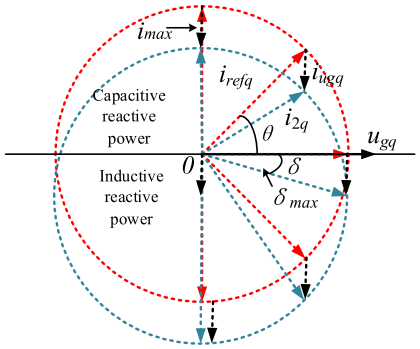

FIGURE 5. Vector diagram of error caused by u_g.

3) INFLUENCE OF THREE INTERNAL DISTURBANCES

As we can see in Fig. 21, the coupled channels will be removed by PI decoupling method at the ideal situation. So if the control parameters are selected reasonably, the PI decoupling method has great robustness for internal disturbances. The d axis is the active current control axis to stabilize DC capacitor voltage. If current signal or voltage signal in d axis is unstable, disturbances will influence q axis via coupled channels. Parameter perturbations of LCL filter also decreases control accuracy of traditional PI decoupling method, which can be caused by complex power grid and old service life [26]. So it is important to consider and analysis the influence of three internal disturbances: $\omega_1 L_1 i_{1d}$, $\omega_1 C u_{cd}$, $\omega_1 L_2 i_{2d}$. $\omega_1 L_2 i_{2d}$ has the same influence with u_{gq} because of the same disturbance position. Closed-loop transfer functions from $\omega_1 L_1 i_{1d}$ to i_{2q} and from $\omega_1 C u_{cd}$ to i_{2q} are shown in (6) and (7) respectively.

$$D_{i1d}(s) = -\frac{R_c s}{R_c C L_1 L_2 s^4 + L_1 L_2 s^3 + R_c (L_1 + L_2) s^2 + R_c G_{inv} K_p s + R_c G_{inv} K_i} \quad (6)$$

$$D_{ucd}(s) = -\frac{R_c L_1 s^2}{R_c C L_1 L_2 s^4 + L_1 L_2 s^3 + R_c (L_1 + L_2) s^2 + R_c G_{inv} K_p s + R_c G_{inv} K_i} \quad (7)$$

The same simplified method from (4) to (5) is used to (6) and (7). (8) and (9) can be derived. $\omega_1 L_2 i_{2d}$ will cause the same influence as u_{gq} too. The $\omega_1 C u_{cd}$ can cause influence on the amplitude of i_{2q}, not on the phase.

$$D_{i1d\_simple}(s=j2\pi f_1) = -\frac{s}{G_{inv}K_i}|_{s=j2\pi f_1} = -\frac{j2\pi f_1}{G_{inv}K_i} \quad (8)$$

$$D_{ucd\_simple}(s=j2\pi f_1) = -\frac{L_1 s^2}{G_{inv}K_i}|_{s=j2\pi f_1} = \frac{4\pi^2 f_1^2 L_1}{G_{inv}K_i} \quad (9)$$

Based on the above analysis, the influence of internal and external disturbances on LCL-type STATCOM with PI decoupling method should not be ignored any more. ADRC decoupling method has better performance to suppress these disturbances, which will be introduced next.

III. APPLICATION OF ADRC TO LCL-TYPE STATCOM

A. CONTROL MODEL OF LCL-TYPE STATCOM WITH ADRC

The analyses in section II show that the traditional PI decoupling method has many problems under the influence of disturbances. These problems include poor reactive compensation performance and instability. ADRC provides a great solution, it is an advanced controller which is different from the traditional PI controller. The advantages of ADRC are introduced in section I.

Taking the LCL-type STATCOM as the research object. By estimating and compensating the internal and external disturbances for q axis current control. ADRC decoupling method can decouple the block diagram shown in Fig. 2 into two 3-order integral units that do not affect each other, this will be introduced next. The performance to reject the disturbances of u_g and L_g is improved. 3-order ADRC is applied since the LCL filter is a 3-order system. According to (2), 3-order differentials of i_{2d} and i_{2q} are derived:

$$\begin{cases} \dfrac{d^3 i_{2d}}{dt^3} = b u_{id} + f_d \\ \dfrac{d^3 i_{2q}}{dt^3} = b u_{iq} + f_q, \end{cases} \qquad b = \frac{1}{CL_1 (L_2 + L_g)} \quad (10)$$

Actually, we control i_2 by adjusting the amplitude and phase of u_i. But the "total disturbances" f_d and f_q shown in (A1), as shown at the bottom of page 9, will cause bad influence on output current control. It can be known from the parameter b, L_g can cause bad influence on output current control too. In order to achieve a better compensation effects, it is necessary to find a parameter b_0 for ADRC that can accurately estimate and compensate b, which will be introduced later.

Compared with nonlinear ADRC, linear ADRC needs fewer tuning control parameters, it has more practical application value. Because the LCL-type STATCOM is a time-delay system, the differential tracker (TD) contained in the traditional ADRC can be ignored. Linear expansion state observer (LESO) and linear state error feedback controller (LSEF) are introduced next.

1) LINEAR EXPANSION STATE OBSERVER (LESO)

As the core part of ADRC, the LESO with excellent performance can always accurately estimate the state variables

and disturbances of the controlled system. The 4-order matrix (11) is derived by (2) and (10).

$$\begin{cases} \begin{bmatrix} \frac{di_{2q}}{dt} \\ \frac{d^2i_{2q}}{dt^2} \\ \frac{d^3i_{2q}}{dt^3} \\ \frac{df_q}{dt} \end{bmatrix} = \begin{bmatrix} 0 & 1 & 0 & 0 \\ 0 & 0 & 1 & 0 \\ 0 & 0 & 0 & 1 \\ 0 & 0 & 0 & 0 \end{bmatrix} \begin{bmatrix} i_{2q} \\ \frac{di_{2q}}{dt} \\ \frac{d^2i_{2q}}{dt^2} \\ f_q \end{bmatrix} + \begin{bmatrix} 0 & 0 \\ 0 & 0 \\ b & 0 \\ 0 & 1 \end{bmatrix} \begin{bmatrix} u_{iq} \\ \frac{df_q}{dt} \end{bmatrix} \\ y = \begin{bmatrix} 1 & 0 & 0 & 0 \end{bmatrix} \begin{bmatrix} i_{2q} & \frac{di_{2q}}{dt} & \frac{d^2i_{2q}}{dt^2} & f_q \end{bmatrix}^T \end{cases} \tag{11}$$

The 4-order LESO is chosen according to the controlled system. According to (11), the LESO is derived and given as follows:

$$\begin{bmatrix} \dot{z}_1 \\ \dot{z}_2 \\ \dot{z}_3 \\ \dot{z}_4 \end{bmatrix} = \begin{bmatrix} -\beta_1 & 1 & 0 & 0 \\ -\beta_2 & 0 & 1 & 0 \\ -\beta_3 & 0 & 0 & 1 \\ -\beta_4 & 0 & 0 & 0 \end{bmatrix} \begin{bmatrix} z_1 \\ z_2 \\ z_3 \\ z_4 \end{bmatrix} + \begin{bmatrix} 0 & \beta_1 \\ 0 & \beta_2 \\ b_0 & \beta_3 \\ 0 & \beta_4 \end{bmatrix} \begin{bmatrix} u_q \\ i_{2q} \end{bmatrix} \tag{12}$$

where, b_0 is compensation factor, it can be used to estimate b shown in (10); β_{1-4} is observer parameters of ADRC.

2) LINEAR STATE ERROR FEEDBACK CONTROLLER (LSEF)

The LSEF is the control core of ADRC. Under the premise of LESO's accurate estimate of disturbances and state variables, LSEF can be designed as a proportional controller. Fig. 22 shows the ADRC current decoupling method and PI current decoupling method for LCL-type STATCOM. As we see in Fig. 21, there are more complex decoupled channels for PI decoupling method. Many sampling sensors are needed too, which will increase the cost. The reference value of d axis current inner-loop control comes from the output of DC capacitor voltage outer-loop. The reference value of q axis current inner-loop control comes from the output of PCC voltage outer-loop.

$$\begin{cases} \frac{d^3i_{2q}}{dt^3} = (f_q - z_4) + u_o \approx u_o \\ u_o = K_{p1}\left(i_{refq} - z_1\right) - K_{p2}z_2 - K_{p3}z_3 \\ \frac{u_{iq}}{G_{inv}} = u_q = \frac{(u_o - z_4)}{b_0} \end{cases} \tag{13}$$

Since the triangular carrier wave amplitude of SPWM can be selected appropriately at the actual debugging process, G_{inv} takes the value of 1 for simplify analysis next. Where, K_{p1-3} are control parameters of LESO, which can directly affect the control performance of ADRC.

B. EFFECT ANALYSIS OF ADRC ON LCL-TYPE STATCOM

If the parameters β_{1-4} and K_{p1-3} are chosen properly. z_{1-4} can estimate i_{2q}, the differential of i_{2q}, the 2-order differential of i_{2q}, and $f_q$perfectly. The coupled system shown in Fig. 2 will be transformed into two same ideal 3-order systems. At the same time, according to the third equation in (13), the "total disturbances" f_q can be compensated by LSEF. According to the first two equations in (13), transfer function (14) can be derived by *Laplace* transformation.

$$\frac{i_{2q}}{i_{refq}} = \frac{K_{p1}}{s^3 + K_{p3}s^2 + K_{p2}s + K_{p1}} \tag{14}$$

Under the non-ideal situation, in order to consider the influence of disturbances on control performance, we change (12) to (15) and substitute (15) to (13), u_{iq} shown in (A2), as shown at the bottom of page 9, can be derived. Where, $\boldsymbol{A}(s)$ and $M(s)$ are shown in (16), A_{1-4} are the first column elements of $\boldsymbol{A}(s)$; B_{1-4} are the second column elements of $\boldsymbol{A}(s)$.

$$\begin{bmatrix} z_1 & z_2 & z_3 & z_4 \end{bmatrix}^T = \frac{\boldsymbol{A}(s)}{M(s)} \begin{bmatrix} u_{iq} \\ i_{2q} \end{bmatrix} \tag{15}$$

According to (A2), the decoupled control block diagram of q axis can be derived, which is shown in Fig. 6.

$$\begin{cases} \boldsymbol{A}(s) = \begin{bmatrix} b_0 s & \beta_1 s^3 + \beta_2 s^2 + \beta_3 s + \beta_4 \\ b_0 s^2 + b_0\beta_1 s & \beta_2 s^3 + \beta_3 s^2 + \beta_4 s \\ b_0 s^3 + b_0\beta_1 s^2 + b_0\beta_2 s & \beta_3 s^3 + \beta_4 s^2 \\ -b_0\beta_4 & \beta_4 s^3 \end{bmatrix} \\ M(s) = s^4 + \beta_1 s^3 + \beta_2 s^2 + \beta_3 s + \beta_4 \end{cases} \tag{16}$$

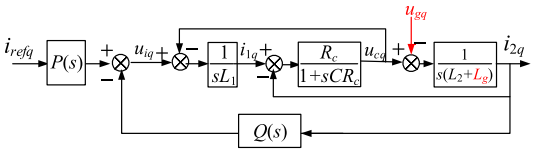

FIGURE 6. The control block diagram of q axis after ADRC decoupling.

According to the analysis in section II, there is no inhibited effect for PI decoupling method on the grid inductance L_g. However, when the control parameters are improperly selected, unstable situations will occur.

$$\begin{cases} \beta_1 = 4\omega_o,\ \beta_2 = 6\omega_o^2,\ \beta_3 = 4\omega_o^3,\ \beta_4 = \omega_o^4 \\ K_{p1} = \omega_c^3,\ K_{p2} = 3\omega_c^2,\ K_{p3} = 3\omega_c \end{cases} \tag{17}$$

According to [27], the control parameters of the ADRC can be selected by referring controller bandwidth ω_c and observer bandwidth ω_o. The reference relationship can be summarized as shown in (17). We take the values that: $\omega_c = 6600$ and $\omega_o = 9600$. The control parameters are shown in Table 2. It should be noted that b_0 with 10 power is changeable and follows with L_g.

1) ROBUSTNESS IMPROVEMENT FOR POWER GRID INDUCTANCE

The filter parameters shown in Table 1 are used to study the influence of L_g on the stability of the STATCOM. According to Fig. 6, the transfer function from i_{refq} to i_{2q} is shown in (18). Based on (3) and (18), pole-zero map is shown in Fig. 7. When L_g is changed, the positions of the poles are

TABLE 2. Parameters of ADRC decoupling method.

Parameter/Unit	Value	Parameter/Unit	Value
LESO parameter β_1	3.84×10^4	LSEF parameter K_{p1}	2.9×10^{11}
LESO parameter β_2	5.5×10^8	LSEF parameter K_{p2}	1.3×10^8
LESO parameter β_3	3.5×10^{12}	LSEF parameter K_{p3}	1.98×10^4
LESO parameter β_4	8.5×10^{15}	Parameter b_0	$\times10^{10}$

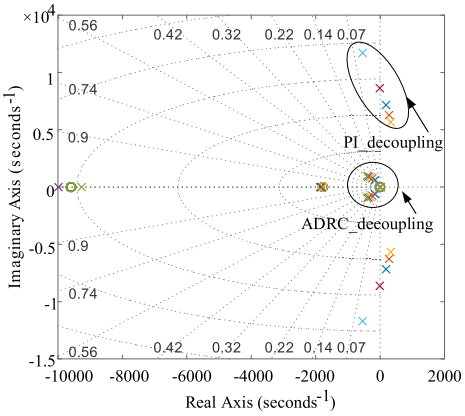

FIGURE 7. Comparison the robustness of L_g of two different decoupling method.

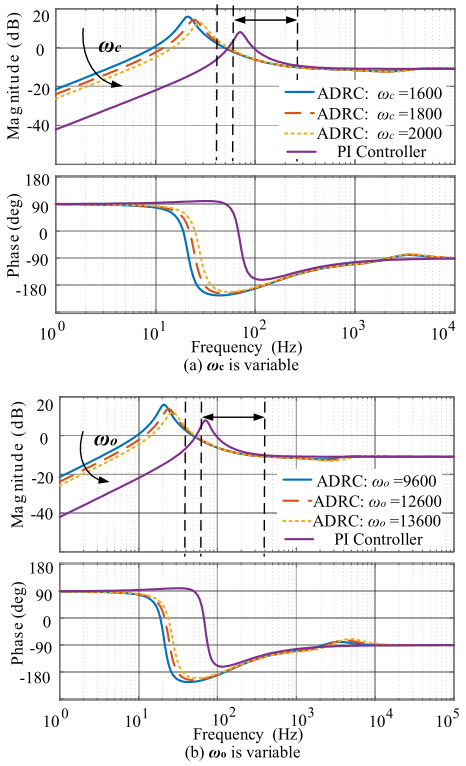

FIGURE 8. Comparison of robustness of u_g under two different decoupling method.

almost unchanged using ADRC decoupling method, and the positions never enter the unstable region, which reflects the disturbance rejection performance.

$$\frac{i_{2q}}{i_{refq}} = \frac{R_cP}{R_cCL_1\left(L_2+L_g\right)s^3+L_1\left(L_2+L_g\right)s^2+R_c\left(L_1+L_2+L_g\right)s+R_cQ} \tag{18}$$

2) ROBUSTNESS IMPROVEMENT FOR HARMONIC POWER GRID VOLTAGE

According to Fig. 6, the transfer function from u_{gq} to i_{2q} is derived in (19). The simplified transfer function is obtained in (20) by ignoring the items with small magnitude. Bode diagrams of (4) and (19) are shown in Fig. 8. The robustness of ADRC decoupling method for grid voltage can be improved by selecting suitable control parameters. The suppression of ADRC decoupling method for lower-order harmonic grid voltage is better.

$$\frac{i_{2q}}{u_{gq}} = -\frac{R_cCL_1s^2+L_1s+R_c}{R_cCL_1L_2s^3+L_1L_2s^2+R_c\left(L_1+L_2\right)s+R_cQ} \tag{19}$$

$$\begin{cases} \dfrac{i_{2q}}{u_{gq}}|_{ADRC\_simple} = -\dfrac{L_1s+R_c}{R_c\left(L_1+L_2\right)s+R_cQ} \\ \dfrac{i_{2q}}{u_{gq}}|_{PI\_simple} = -\dfrac{L_1s^2+R_cs}{R_c\left(L_1+L_2\right)s^2+R_cK_ps+R_cK_i} \end{cases} \tag{20}$$

IV. VERIFICATION BASED ON LCL-TYPE STATCOM SIMULATION MODEL

A. COMPARISION OF ADRC AND PI CONTROLLER

Since the LCL filter is a 3-order system and the control delay can be seen as a 1-order system, in order to study the performance of ADRC decoupling method, a 4-order transfer function $E(s)$ is designed in (21) for verification. PI controller and ADRC are all employed to $E(s)$. Control parameters in Table 1 and Table 2 are used. Fig. 9 shows the comparison result of the unit step response. Since (21) is a controlled system with large inertia damping, there is

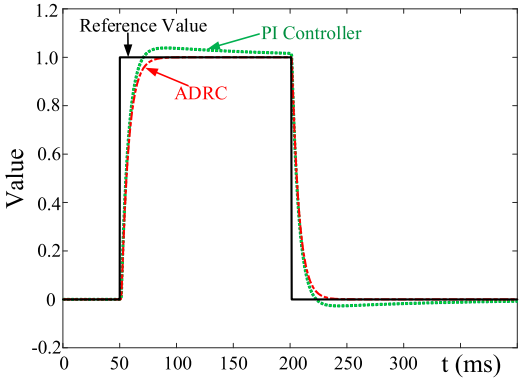

FIGURE 9. Comparison of control effect on 4-order mathematical model (21) based on PI controller and ADRC.

no overshoot in Fig. 9. The dynamic response time of these two controllers is almost the same. But PI controller has longer adjusted time that is almost close to 150ms. On the contrary, ADRC has better performance between response time and adjusted time. The same control parameters are utilized for (22). The comparison result is shown in Fig. 10. As we can see, although there is large overshoot. ADRC has shorter adjusted time and oscillating peak.

$$E(s) = \frac{330}{\left(10.56 \times 10^{-12}s^3 + s\right)\left(1.5 \times 10^{-5}s + 1\right)} \tag{21}$$

$$E(s) = \frac{330}{(10.56\times10^{-12}s^3+5\times10^{-3}s^2+s)(1.5\times10^{-5}s+1)} \tag{22}$$

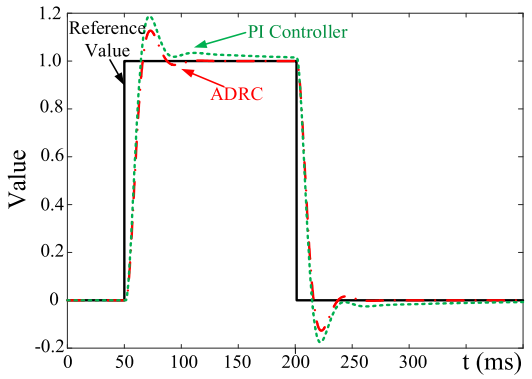

FIGURE 10. Comparison of control effect on 4-order mathematical model (22) based on PI controller and ADRC.

B. CONFIGURATION of LCL-TYPE STATCOM

In order to verify the performance of ADRC decoupling method, a 20kVar LCL-type STATCOM connected to the load side of power grid is built based on MATLAB/Simulink. The results of different working conditions are given next to verify the correctness of theoretical analysis and the feasibility of ADRC decoupling method. Actually, the simulation model and mathematical model are very similar, but still different. The voltage control outer loop is considered in simulation model. So the control parameters should be adjusted slightly. Where, we take the values that: $\omega_c = 13000$ and $\omega_o = 9600$. The parameters of reactive compensation system are shown in Table 3.

1) WORKING CONDITION 1

Compared with PI controller, ADRC can solve the contradiction between the dynamic response time and overshoot. Sudden fluctuation in load reactive power occurs at time t_1. Based on LCL-type STATCOM model, the control effect comparison of PI decoupling method and ADRC decoupling method is shown in Fig. 11. Where, RMS is the root mean square value of output reactive compensation current i_2. The response time of these two control methods is almost the same, even PI decoupling method is shorter. But the adjusted

TABLE 3. Parameters of 20kVar LCL-type STATCOM.

Parameter/ Unit	Value	Parameter/ Unit	Value
DC capacitor voltage U_{dc}/V	750	DC capacitor C/μF	1500
Swithing frequency f/Hz	50	Capacity of STATCOM Q/kVar	20
Inverter-side inductor L_1/mH	5.5	LSEF parameter b_0	$\times10^{10}$
Gird-side inductor L_2/mH	0.6	LSEF parameter K_{p3}	3.9×10^{4}
Capacitor C/μF	6.6	LSEF parameter K_{p2}	5×10^{8}
Damping resistor R_c/Ω	3	LSEF parameter K_{p1}	2.2×10^{12}
DC voltage controller $K_{p\ dc}$	1	DC voltage controller $K_{i\ dc}$	4
PCC voltage controller $K_{p\ pcc}$	1.5	PCC voltage controller $K_{i\ pcc}$	200
LESO parameter β_1	3.8×10^{4}	LESO parameter β_2	5.5×10^{8}
LESO parameter β_3	3.5×10^{12}	LESO parameter β_4	8.5×10^{15}

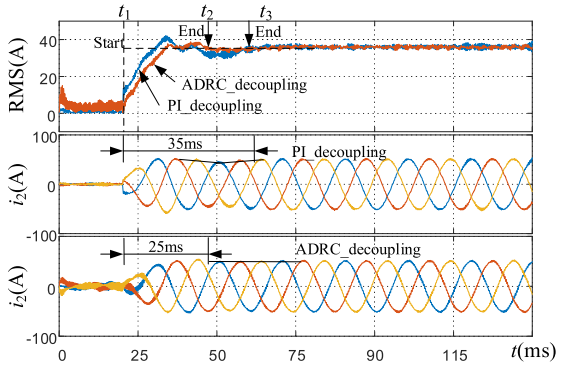

FIGURE 11. Control effect comparison under load reactive power fluctuation.

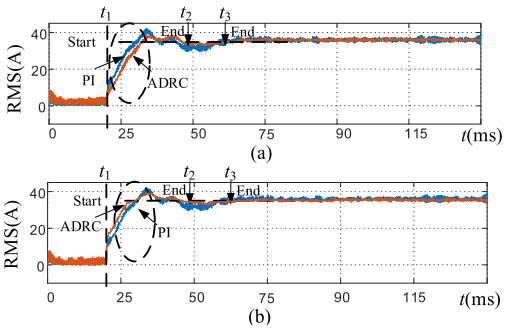

FIGURE 12. Control effect comparison under load reactive power fluctuation. (a) $\omega_o = 10600$; $\omega_c = 15600$. (b) $\omega_o = 12600$; $\omega_c = 16600$.

time of ADRC decoupling method is shorter. The overshoot of ADRC decoupling method is smaller. In order to improve the dynamic response time of ADRC decoupling method, we adjusted control parameters appropriately. The results are shown in Fig. 12. As we can see, better dynamic response performance can be obtained by selecting suitable control parameters.

2) WORKING CONDITION 2

Under the premise of working condition 1, increase the value of L_g from 0mH to 0.8mH, Fig. 13 shows that the THD of i_2 is increased too. The fast Fourier transform results of i_2 are shown in Fig. 14. The THD of i_2 with ADRC decoupling method is smaller. It should be noted that b_0 is changed following with L_g. According to [28], [29], the long distance transmission and parallel multiple grid-connected inverters will increase the value of grid inductance L_g. Although L_g is a variable, it can take the large value at the extreme condition. Increasing the value of L_g from 0.8mH to 1.5mH, i_2 with PI decoupling method will diverge, which is shown in Fig. 15. The STATCOM loses stability under the influence of large grid inductance. In contrast, ADRC decoupling method has stronger robustness when L_g is increased. The results of simulation are consistent with the theoretical analysis.

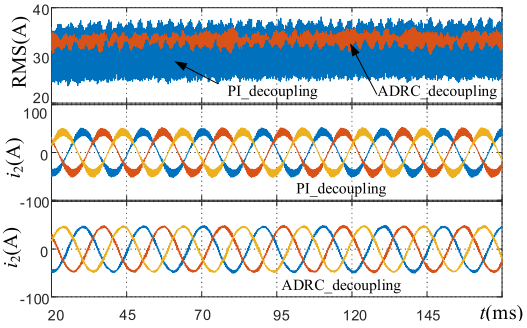

FIGURE 13. Control effect comparison when $L_g = 0.8$mH.

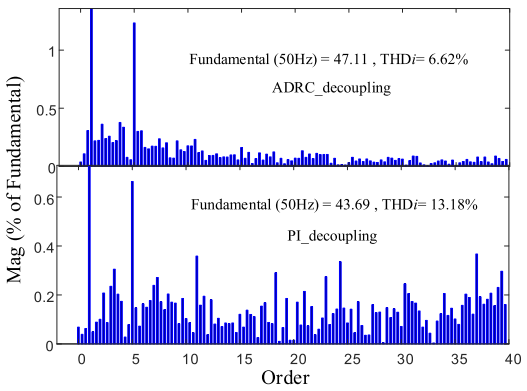

FIGURE 14. Comparison of THD$_i$.

3) WORKING CONDITION 3

Because the d axis is mainly used to keep the DC capacitor voltage stability, the fluctuations of current and voltage in d axis will occur frequently. Actually, the internal disturbances from coupled channels are difficult to measure. We only need to verify the robustness of ADRC decoupling method to suppose these disturbances. Supposing that $\omega_1 L_1 i_{1d} = +20$A at t_1 and $\omega_1 L_1 i_{1d} = -20$A at t_2 in Fig. 16 and Fig. 17, it can be found that the PI decoupling method and ADRC decoupling method all have the great

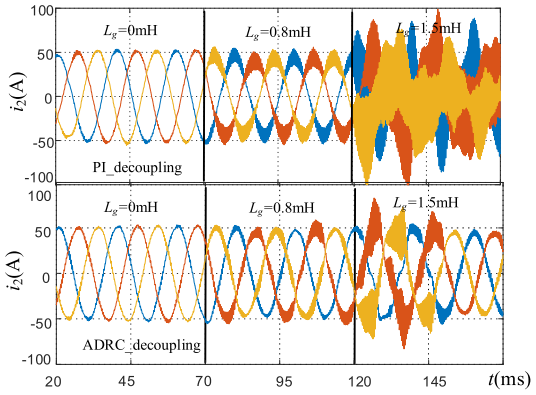

FIGURE 15. Control effect comparison when $L_g = 1.5$mH.

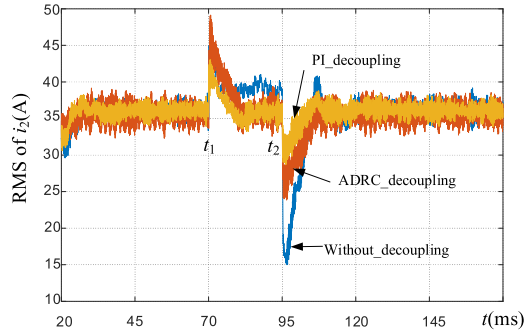

FIGURE 16. Control effect comparison under the influence of coupled channel disturbances. $\omega_o = 10600$; $\omega_c = 13600$.

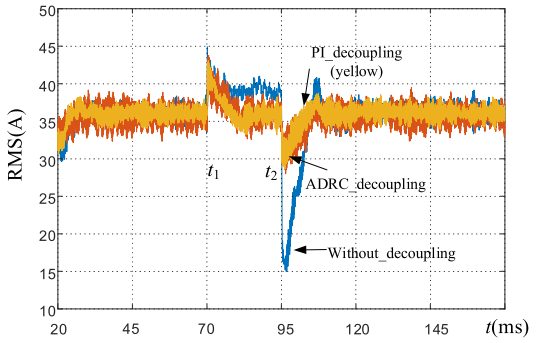

FIGURE 17. Control effect comparison under the influence of coupled channel disturbances. $\omega_o = 11600$; $\omega_c = 14600$.

performance to reject disturbances, because these two methods all can remove the decoupled channels. These methods can restore the STATCOM to normal working state quickly. The oscillation is large under the direct current control without decoupling. The following performance and robustness of ADRC decoupling method are excellent, which are consistent with the theoretical analysis. The different results with different control parameters are shown in Fig. 17. We can find that the disturbance rejection performance can be improved by selecting suitable control parameters. Because the parameters selection isn't the studying focus in this manuscript, the detailed content is omitted.

4) WORKING CONDITION 4

According to IEEE Std.1547-2003, the maximum allowable THD of grid voltage is 5%. In normal, the THD of grid voltage is far lower than 5%. 3-order harmonic grid voltage and 5-order harmonic grid voltage are injected into the fundamental grid voltage in the simulation system. The contents of these gird voltage harmonics are shown in Table 4. According to the analysis in section II, the THD of i_2 will increase under the influence of harmonic grid voltage. The grid voltage feedforward control based on PI controller is shown in Fig. 23. The simulation results are shown in Fig. 18. The ADRC decoupling method and PI feedforward decoupling method can all alleviate the THD of i_2 caused by the harmonic grid voltage. The traditional direct current control doesn't have the harmonic suppression capability, and it leads to an increased THD of i_2, which is shown in Fig. 18(b). The results of simulation are consistent with the theoretical analysis too.

TABLE 4. The contents of harmonic voltage distortion.

Individual harmonic order	h = 1	h = 3	h = 5	Total harmonic distortion
Voltage value (V)	220	6	8	4.5%
% of fundamental voltage	100%	2.7%	3.6%	

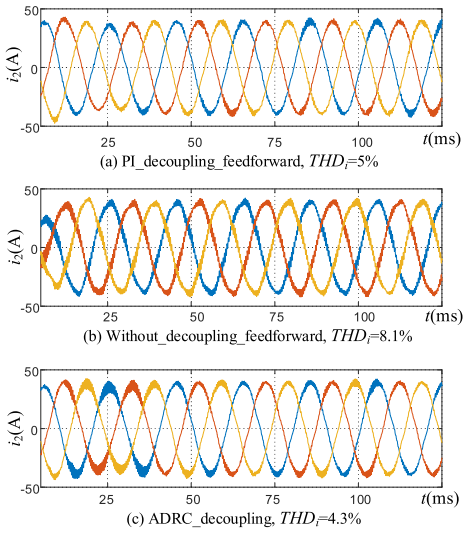

FIGURE 18. Control effect comparison under the influence of harmonic grid voltage.

In order to verify the effectiveness of ADRC decoupling method for different capacity of the STATCOM. We reduce the capacity in simulation. The results are shown in Fig. 19 and Fig. 20. As we can see, the STATCOM has the same robustness to external disturbances too. Because the perfect decoupling lies in control structure and parameters, the robustness for internal disturbance doesn't be influenced by the capacity of the STATCOM. Based on the above simulation results under the different working conditions, the control performance comparisons of the ADRC decoupling method, the PI feedforward decoupling method and the direct current control method are shown in Table 5.

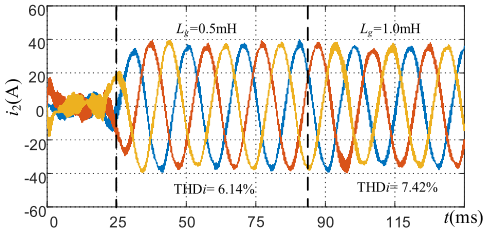

FIGURE 19. Control effect for grid inductance variation under different capacity of STATCOM.

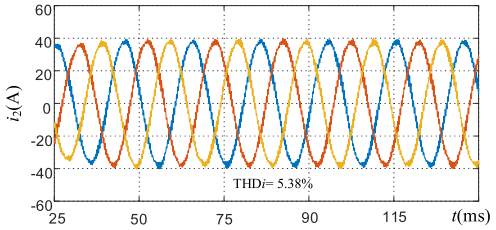

FIGURE 20. Control effect for harmonic grid voltage under different capacity of STATCOM.

V. CONCLUSION

An original current decoupling method with ADRC is proposed in this paper, this method can improve the robustness of LCL-type STATCOM to reject the internal and external disturbances. These disturbances will influence the stability of PI decoupling control and deteriorate the reactive compensation performance of LCL-type STATCOM. Principle analyses about how to apply the ADRC to achieve current decoupling control of STATCOM are given. Based on the mathematical models, the comparison results show that the

$$\begin{cases} f_d = \dfrac{1}{CR_c\left(L_2+L_g\right)}\left(-R_c\dfrac{di_{2d}}{dt}+\dfrac{L_1-CR_c^2}{L_1CR_c}u_{cd}+\dfrac{1}{C}i_{2d}-\dfrac{1}{C}i_{1d}+R_c\omega_1 C\dfrac{du_{cq}}{dt}+\omega_1R_ci_{1q}-\omega_1u_{cq}\right)+\omega_1\dfrac{d^2i_{2q}}{dt^2}-\dfrac{1}{L_2+L_g}\dfrac{d^2u_{gd}}{dt^2} \\ f_q = \dfrac{1}{CR_c\left(L_2+L_g\right)}\left(-R_c\dfrac{di_{2q}}{dt}+\dfrac{L_1-CR_c^2}{L_1CR_c}u_{cq}+\dfrac{1}{C}i_{2q}-\dfrac{1}{C}i_{1q}-R_c\omega_1 C\dfrac{du_{cd}}{dt}-\omega_1R_ci_{1d}+\omega_1u_{cd}\right)-\omega_1\dfrac{d^2i_{2d}}{dt^2}-\dfrac{1}{L_2+L_g}\dfrac{d^2u_{gq}}{dt^2} \end{cases} \tag{A1}$$

$$u_{iq} = Pi_{ief} - Qi_{2q} = \frac{MK_{p1}}{b_0M+K_{p1}A_1+K_{p2}A_2+K_{p3}A_3+A_4}i_{ief} - \frac{K_{p1}B_1+K_{p2}B_2+K_{p3}B_3+B_4}{b_0M+K_{p1}A_1+K_{p2}A_2+K_{p3}A_3+A_4}i_{2q} \tag{A2}$$

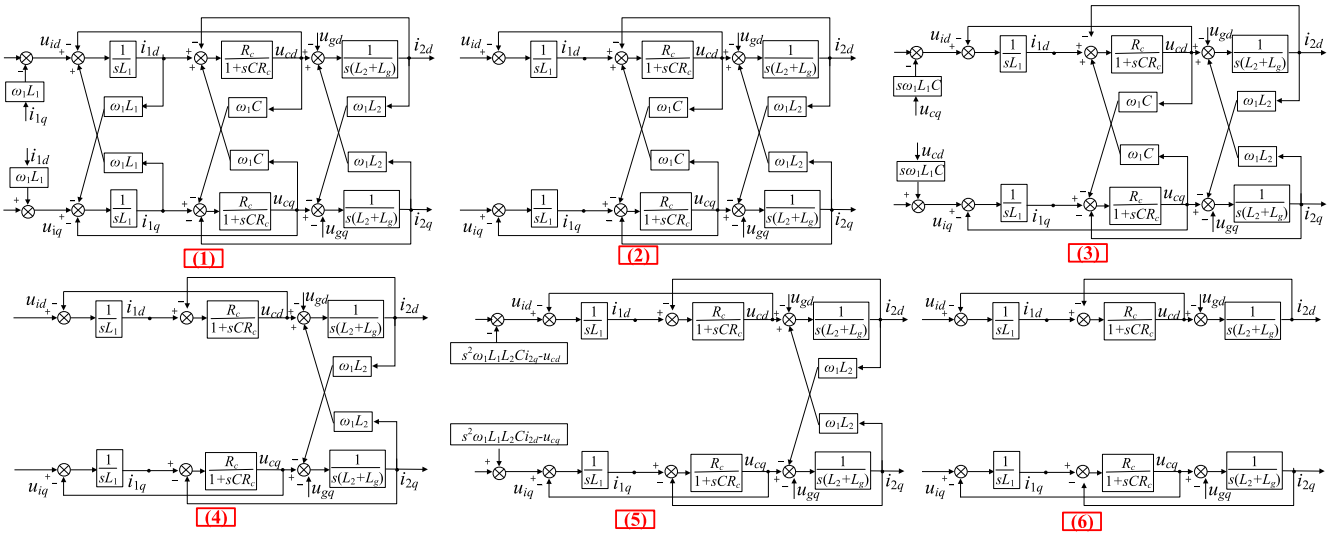

FIGURE 21. PI decoupling method.

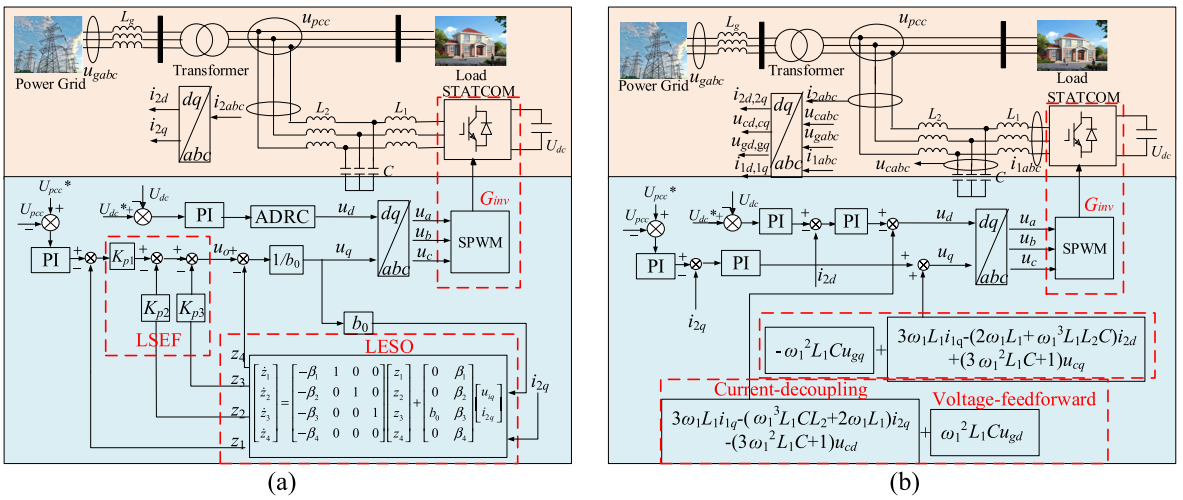

FIGURE 22. Block diagram of LCL-type STATCOM, (a) ADRC decoupling method. (b) PI decoupling method with voltage feedforward.

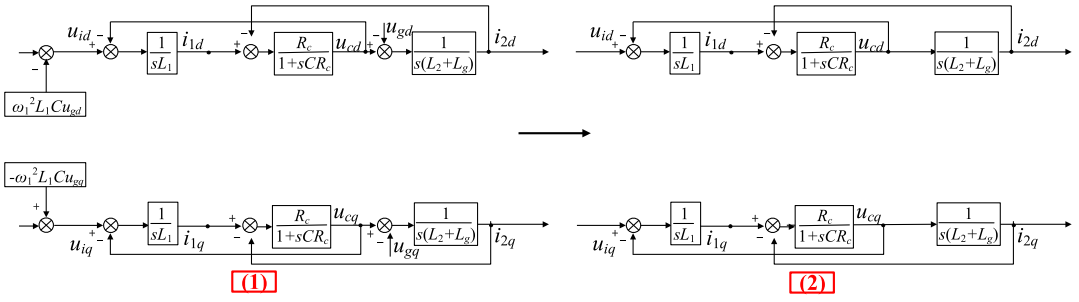

FIGURE 23. Voltage feedforward control method.

method proposed in this paper has higher robustness than PI decoupling method under the influence of grid inductance variation. At the same time, ADRC decoupling method can reject internal disturbances by removing coupled channels between d axis and q axis, and it also has high robustness to harmonic grid voltage. The results from a LCL-type STATCOM simulation models are consisted with the theoretical analyses. The effectiveness and superiority of ADRC

TABLE 5. Performance comparisons of different control method.

Control method	Complex	Cost	Dynamic response	Robustness (internal disturbance)	Robustness (external disturbance)	Stability	Depending on accurate model of controlled system?
ADRC decoupling [25]	**	*	***	***	***	***	No
PI feedforward decoupling [8], [20]-[22]	***	***	***	***	**	**	Yes
direct current control [17]-[19]	*	**	**	*	*	*	Yes

decoupling method are verified too. According to multiple performance indicators shown in Table 5, ADRC decoupling method has higher application value and better industrial application prospects.

APPENDIX

See (A1) and (A2), Figs. 21–23, and Table 5.

REFERENCES

[1] L. Wang, C.-H. Chang, B.-L. Kuan, and A. V. Prokhorov, "Stability improvement of a two-area power system connected with an integrated onshore and offshore wind farm using a STATCOM," *IEEE Trans. Power Syst.*, vol. 53, no. 2, pp. 867–877, Apr. 2017.

[2] D. Lu, J. Zhu, J. Wang, J. Yao, S. Wang, and H. Hu, "A simple zero-sequence-voltage-based cluster voltage balancing control and the negative sequence current compensation region identification for star-connected cascaded H-bridge STATCOM," *IEEE Trans. Power Electron.*, vol. 33, no. 10, pp. 8376–8387, Oct. 2018.

[3] L. Hao, S. Hanliang, X. Liancheng, L. Anling, and Z. Bin, "Coordination control of positive and negative sequence voltages of cascaded H-bridge STATCOM operating under imbalanced grid voltage," *J. Eng.*, vol. 2019, no. 16, pp. 2743–2747, Mar. 2018.

[4] J. Xu, S. Xie, Q. Qian, and B. Zhang, "Adaptive feedforward algorithm without grid impedance estimation for inverters to suppress grid current instabilities and harmonics due to grid impedance and grid voltage distortion," *IEEE Trans. Ind. Electron.*, vol. 64, no. 9, pp. 7574–7586, Sep. 2017.

[5] X. Chen, Y. Zhang, S. Wang, J. Chen, and C. Gong, "Impedance-phased dynamic control method for grid-connected inverters in a weak grid," *IEEE Trans. Power Electron.*, vol. 32, no. 1, pp. 274–283, Jan. 2017.

[6] X. Li, J. Fang, Y. Tang, X. Wu, and Y. Geng, "Capacitor-voltage feed-forward with full delay compensation to improve weak grids adaptability of LCL-filtered grid-connected converters for distributed generation systems," *IEEE Trans. Power Electron.*, vol. 33, no. 1, pp. 749–764, Jan. 2018.

[7] Y. He, H. S.-H. Chung, C.-T. Lai, X. Zhang, and W. Wu, "Active cancelation of equivalent grid impedance for improving stability and injected power quality of grid-connected inverter under variable grid condition," *IEEE Trans. Power Electron.*, vol. 33, no. 11, pp. 9387–9398, Nov. 2018.

[8] S. Zhou, J. Liu, L. Zhou, and Y. Zhang, "DQ current control of voltage source converters with a decoupling method based on preprocessed reference current feed-forward," *IEEE Trans. Power Electron.*, vol. 32, no. 11, pp. 8904–8921, Nov. 2017.

[9] J. Han, "From PID to active disturbance rejection control," *IEEE Trans. Ind. Electron.*, vol. 56, no. 3, pp. 900–906, Mar. 2009.

[10] L. Cheng, M. Chen, and Z. Li, "Design and control of a wearable hand rehabilitation robot," *IEEE Access*, vol. 6, pp. 74039–74050, 2018.

[11] Z. Ma, Y. Fang, H. Zheng, and L. Liu, "Active disturbance rejection control with self-adjusting parameters for vibration displacement system of continuous casting mold," *IEEE Access*, vol. 7, pp. 52498–52507, 2019.

[12] S. Li and J. Li, "Output predictor-based active disturbance rejection control for a wind energy conversion system with PMSG," *IEEE Access*, vol. 5, pp. 5205–5214, 2017.

[13] N. Yang, F. Gao, D. Paire, A. Miraoui, and W. Liu, "Distributed control of multi-time scale DC microgrid based on ADRC," *IET Power Electron.*, vol. 10, no. 3, pp. 329–337, Sep. 2016.

[14] Y. Zuo, X. Zhu, L. Quan, C. Zhang, Y. Du, and Z. Xiang, "Active disturbance rejection controller for speed control of electrical drives using phase-locking loop observer," *IEEE Trans. Ind. Electron.*, vol. 66, no. 3, pp. 1748–1759, Mar. 2019.

[15] R. Zhou and W. Tan, "Analysis and tuning of general linear active disturbance rejection controllers," *IEEE Trans. Ind. Electron.*, vol. 66, no. 7, pp. 5497–5507, Jul. 2019.

[16] C. Kang, S. Wang, W. Ren, Y. Lu, and B. Wang, "Optimization design and application of active disturbance rejection controller based on intelligent algorithm," *IEEE Access*, vol. 7, pp. 59862–59870, 2019.

[17] X. Zhang, L. Tan, J. Xian, H. Zhang, Z. Ma, and J. Kang, "Direct grid-side current model predictive control for grid-connected inverter with LCL filter," *IEEE Trans. Power Electron.*, vol. 11, no. 15, pp. 2450–2460, Dec. 2018.

[18] Y.-Y. Hong and M.-J. Liu, "Optimized interval type-II fuzzy controller-based STATCOM for voltage regulation in power systems with photovoltaic farm," *IEEE Access*, vol. 6, pp. 78731–78739, 2018.

[19] E. Kontos, G. Tsolaridis, R. Teodorescu, and P. Bauer, "High order voltage and current harmonic mitigation using the modular multilevel converter STATCOM," *IEEE Access*, vol. 5, pp. 16684–16692, 2017.

[20] R. Sajadi, H. Iman-Eini, M. K. Bakhshizadeh, Y. Neyshabouri, and S. Farhangi, "Selective harmonic elimination technique with control of capacitive DC-link voltages in an asymmetric cascaded H-bridge inverter for STATCOM application," *IEEE Trans. Ind. Electron.*, vol. 65, no. 11, pp. 8788–8796, Nov. 2018.

[21] G. Farivar, B. Hredzak, and V. G. Agelidis, "Decoupled control system for cascaded H-bridge multilevel converter based STATCOM," *IEEE Trans. Ind. Electron.*, vol. 63, no. 1, pp. 322–331, Jan. 2016.

[22] Y. Yu and X. Hu, "Active disturbance rejection control strategy for grid-connected photovoltaic inverter based on virtual synchronous generator," *IEEE Access*, vol. 7, pp. 17328–17336, 2019.

[23] B. Wang, Z. Shen, H. Liu, and J. Hu, "Linear ADRC direct current control of grid-connected inverter with LCL filter for both active damping and grid voltage induced current distortion suppression," *IET Power Electron.*, vol. 11, no. 11, pp. 1748–1755, Sep. 2018.

[24] J. Yang, H. Cui, S. Li, and A. Zolotas, "Optimized active disturbance rejection control for DC-DC buck converters with uncertainties using a reduced-order GPI observer," *IEEE Trans. Circuits Syst. I, Reg. Papers*, vol. 65, no. 2, pp. 832–841, Feb. 2018.

[25] A. Benrabah, D. Xu, and Z. Gao, "Active disturbance rejection control of LCL-filtered grid-connected inverter using Padé approximation," *IEEE Trans. Ind. Appl.*, vol. 54, no. 6, pp. 6179–6189, Nov. 2018.

[26] Y. Zhao, J. Wang, W. Yao, and J. Zhang, "Current loop controller design of STATCOM based on the new improved internal model decoupling control," *Proc. CSEE*, vol. 37, no. 18, pp. 5409–5419, Sep. 2017.

[27] Z. Gao, "Scaling and bandwidth-parameterization based controller tuning," in *Proc. Amer. Control Conf.*, vol. 6, Jun. 2003, pp. 4989–4996.

[28] M. Ashabani, Y. A.-R. I. Mohamed, M. Mirsalim, and M. Aghashabani, "Multivariable droop control of synchronous current converters in weak grids/microgrids with decoupled DQ-axes currents," *IEEE Trans. Smart Grid*, vol. 6, no. 4, pp. 1610–1620, Jul. 2015.

[29] Q. Qian, S. Xie, L. Huang, J. Xu, Z. Zhang, and B. Zhang, "Harmonic suppression and stability enhancement for parallel multiple grid-connected inverters based on passive inverter output impedance," *IEEE Trans. Ind. Electron.*, vol. 64, no. 9, pp. 7587–7598, Sep. 2017.

MINGLEI WANG was born in Shandong, China, in 1995. He received the B.S. degree in electrical engineering and automation from the Shandong University of Science and Technology, Shandong, in 2018. He is currently pursuing the M.S. degree with the Harbin Institute of Technology. His current research interests include smart grid control, renewable energy, and power quality.

XIANGYU WANG was born in Heilongjiang, China, in 1994. He received the B.S. degree in electrical engineering and automation from the China University of Petroleum, Shandong, China in 2016. He is currently pursuing the M.S. degree with Northeast Petroleum University. His current research interests include model predictive control and sensor-less motor control.

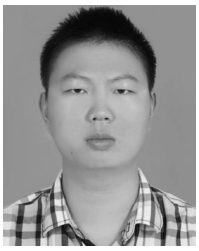

JINXIN QIAO was born in Henan, China, in 1997. He received the B.S. degree in electrical engineering and automation from the Harbin Institute of Technology, Heilongjiang, China, in 2019, where he is currently pursuing the M.S. degree. His current research interests include smart grid control and power quality in the wind farm.

LIGUO WANG was born in Heilongjiang, China, in 1972. He received the B.S. degree from the Harbin University of Science and Technology, Harbin, China, in 1994, and the M.S. and Ph.D. degrees in electrical engineering from the Harbin Institute of Technology, in 1999 and 2002, respectively. In 2015, he was a Visiting Scholar with the School of Electrical and Computer Engineering, Cornell University, Ithaca, NY, USA. Since 2003, he has been with the Department of Electrical and Electronics Engineering, Harbin Institute of Technology, where he is currently a Professor. His current research interests include sensor-less motor control, nonlinear control theory, and smart grids.